

Glass-forming ability and crystallization behavior of $\text{Co}_{62-x}\text{Fe}_x\text{Nb}_6\text{Zr}_2\text{B}_{30}$ ($x=0,16$) amorphous alloys with large supercooled liquid region

J. M. Borrego, C. F. Conde, A. Conde, S. Roth, H. Grahl, A. Ostwald, and J. Eckert

Citation: *Journal of Applied Physics* **92**, 6607 (2002); doi: 10.1063/1.1518768

View online: <http://dx.doi.org/10.1063/1.1518768>

View Table of Contents: <http://scitation.aip.org/content/aip/journal/jap/92/11?ver=pdfcov>

Published by the [AIP Publishing](#)

Articles you may be interested in

[Predicted glass-forming ability of Cu-Zr-Co alloys and their crystallization behavior](#)

J. Appl. Phys. **113**, 123505 (2013); 10.1063/1.4798294

[Abnormal behavior of supercooled liquid region in bulk-forming metallic glasses](#)

J. Appl. Phys. **108**, 053515 (2010); 10.1063/1.3465310

[A criterion for evaluating glass-forming ability of alloys](#)

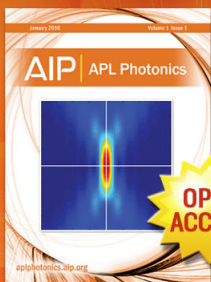
J. Appl. Phys. **106**, 094902 (2009); 10.1063/1.3255952

[Two-stage-like glass transition and the glass-forming ability of a soft magnetic Fe-based glassy alloy](#)

J. Appl. Phys. **105**, 053518 (2009); 10.1063/1.3080139

[Glass-forming ability and soft magnetic properties of FeCoSiAlGaPCB amorphous alloys](#)

J. Appl. Phys. **92**, 2073 (2002); 10.1063/1.1494848



Launching in 2016!

The future of applied photonics research is here

**OPEN
ACCESS**

AIP | APL
Photonics

Glass-forming ability and crystallization behavior of $\text{Co}_{62-x}\text{Fe}_x\text{Nb}_6\text{Zr}_2\text{B}_{30}$ ($x=0,16$) amorphous alloys with large supercooled liquid region

J. M. Borrego, C. F. Conde, and A. Conde^{a)}

Departamento de Física de la Materia Condensada, Instituto de Ciencia de Materiales, C.S.I.C., Universidad de Sevilla, P.O. Box 1065, 41080 Sevilla, Spain

S. Roth, H. Grahl, A. Ostwald, and J. Eckert

Leibniz Institut für Metallische Werkstoffe, IFW, Dresden, Postfach 270016, D-01171 Dresden, Germany

(Received 5 June 2002; accepted 11 September 2002)

The kinetics of the glass transition and the crystallization process of $\text{Co}_{62-x}\text{Fe}_x\text{Nb}_6\text{Zr}_2\text{B}_{30}$ ($x=0,16$) amorphous alloys with large supercooled liquid region was investigated by differential scanning calorimetry. The dependence of the glass transition on the heating rate was analyzed in terms of the Vogel–Fulcher–Tammann equation. The glass-forming ability of these alloys is discussed with respect to the width of the supercooled liquid region, the reduced glass transition temperature, and the fragility parameter. The studied alloys are found to be rather strong glass formers. The crystalline phases formed after the devitrification are identified by means of x-ray diffraction and thermomagnetic measurements. The complicated crystallization process requiring long-range atomic rearrangements seems to contribute to the high stability of the supercooled liquid against crystallization. © 2002 American Institute of Physics. [DOI: 10.1063/1.1518768]

I. INTRODUCTION

The development of Fe- and Co-based amorphous soft magnetic materials with low critical cooling rate for glass formation and a wide supercooled liquid region before crystallization has become an important research topic in recent years.^{1,2} Besides their technological importance due to the combination of high glass-forming ability and good soft magnetic properties, such alloys are excellent materials to study the dynamic behavior of supercooled metallic liquids. Fe–Co–M–B ($M=\text{Zr},\text{Hf},\text{Nb},\text{Ta}$) alloys can be considered as one of the most important systems in which Fe-based bulk glassy alloys with good soft magnetic properties are obtained.^{3,4} The increase in B content up to 30 at. % in (Fe,Co)–(Nb,Zr)–B amorphous alloys causes a large extension of the supercooled liquid region before crystallization^{5,6} making these alloys especially suitable for the study of the kinetics of the glass transition. The kinetic nature of the glass transition provides a means of analyzing the dynamic changes in the supercooled liquid state from the heating rate dependence of the glass transition and therefore, can provide complementary information about the glass-forming ability of the studied systems. It has been reported that alloys with high glass-forming ability, that is, low critical cooling rate for glass formation, are stronger metallic glass formers in the Angell plot⁷ than less thermally stable metallic liquids.⁸

In this article, the effect of Fe addition on the glass-forming ability of $\text{Co}_{62-x}\text{Fe}_x\text{Nb}_6\text{Zr}_2\text{B}_{30}$ ($x=0, 15$) alloys is discussed in terms of several parameters: the width of the supercooled liquid region, the reduced glass transition temperature and the fragility parameter. The dependence of the

glass transition temperature on the heating rate is analyzed in terms of the Vogel–Fulcher–Tanamann (VFT) equation, and the value of the fragility parameter is discussed in the frame of the general classification scheme of glass-forming liquids.^{7,9} The characterization of the crystalline phases formed after the first crystallization step was made by means of x-ray diffraction and thermomagnetic measurements.

II. EXPERIMENTAL PROCEDURE

Multicomponent $\text{Co}_{62-x}\text{Fe}_x\text{Nb}_6\text{Zr}_2\text{B}_{30}$ ($x=0, 16$) alloys ingots were prepared from high purity elements by arc-melting under argon atmosphere. From these pre-alloys, 10-mm-wide and 25- μm -thick ribbons were prepared by the single-roller melt-spinning technique. The samples were proven to be fully amorphous in the as-quenched state by x-ray diffraction (XRD) measurements. X-ray diffraction patterns were recorded at room temperature using a Philips PW 1820 diffractometer with Co K_α radiation. The values of the onset glass transition temperature T_g , the onset crystallization temperature T_x , and the crystallization peak temperature T_p , were determined by differential scanning calorimetry (DSC). The onset glass transition was defined as the point of intersection between the linearly extrapolated curve below the transition with the steepest tangent of the rise in heat flow signal.¹⁰ The experiments were performed with a Perkin-Elmer DSC-7 calorimeter under a continuous argon flow at different heating rates ranging from 0.02 to 2.67 K/s. The crystallization and melting behavior study up to 1700 K was carried out using a Netzsch 404 DSC equipment at a heating rate of 0.17 K/s (10 K/min). The liquidus temperature T_l was determined as the inflection point of the last endotherm of the heating curve (high temperature side).

^{a)}Electronic mail: conde@us.es

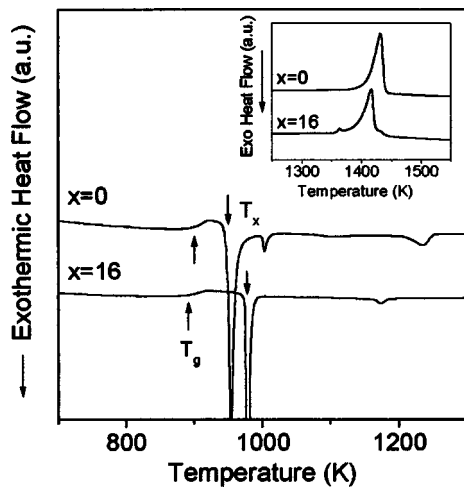


FIG. 1. DSC curves for as-quenched samples of $\text{Co}_{62-x}\text{Fe}_x\text{Nb}_6\text{Zr}_2\text{B}_{30}$ ($x=0,16$) alloys at a heating rate of 0.17 K/s. The inset shows the melting behavior recorded at the same heating rate.

The magnetization as a function of the temperature $M(T)$, was measured with a Faraday magnetometer in a field of 460 kA m^{-1} . Values of the Curie temperature T_C , of the amorphous and crystalline phases were determined by the intersection point of the steepest tangent to the $M(T)$ curve with the T axis or with the magnetization curve extrapolated down temperatures $T < T_C$, respectively.

The coercive field H_c , and the saturation magnetostriction constant λ_s , were measured at room temperature with a Förster Koerzimat and by the small-angle rotation method after Narita *et al.*¹¹ at 15 kA m^{-1} , respectively. The saturation magnetization at room temperature was measured with a vibrating sample magnetometer, using a maximum field strength of 1500 kA m^{-1} .

III. RESULTS AND DISCUSSION

The constant-rate heating differential scanning calorimetry curves for the $\text{Co}_{62x}\text{Fe}_x\text{Nb}_6\text{Zr}_2\text{B}_{30}$ ($x=0,16$) as-quenched alloys recorded at a heating rate of 0.17 K/s are shown in Fig. 1. A distinct glass transition, followed by a large supercooled liquid region, is observed in the temperature range prior to crystallization. Previous to the glass transition, a broad exothermic event can be observed for the two alloys due to structural relaxation. The crystallization process of the Fe-free alloy is evidenced by two main exothermic peaks, while only one significant peak is observed in the alloy containing 16 at. % Fe. The T_g value of about 900 K for the alloy with $x=0$, decreases with the substitution of Co by Fe down to a value of 892 K. On the contrary, the crystallization onset temperature of the alloy with $x=16$ is about

30 K higher than that of the alloy with $x=0$ (see Table I). As a result, the width of the supercooled liquid region estimated from the glass transition onset temperature and the crystallization onset temperature as $\Delta T_x (= T_x - T_g)$, increases from 50 K for the alloy with $x=0$, to 88 K for $x=16$. The wide supercooled liquid region of these multicomponent alloys makes them especially interesting for studying the kinetic behavior of the supercooled liquid.

The inset in Fig. 1 shows the melting behavior of the two alloys as observed by DSC measurements taken at a heating rate of 0.17 K/s. The curve corresponding to the Fe-free alloy exhibits a sharp single melting event indicative of an eutectic composition, while the curve corresponding to the alloy with $x=16$ exhibits a melting behavior very near to the eutectic point. The reduced glass transition temperature of these alloys, T_{rg} , was determined using the relation T_g/T_l (T_l , liquidus temperature) since it was found that T_{rg} defined in this way shows a stronger correlation with the critical cooling rate for glass formation than T_g/T_m (T_m , solidus temperature).¹² According to Turnbull's analysis,¹³ a liquid with $T_{rg} \geq 2/3$ can only crystallize within a very narrow temperature range, and thus can be easily undercooled at a low cooling rate into the glassy state. The calculated value of T_{rg} of about 0.63 for both alloys (Table I), that is, close to $2/3$, indicates that these systems can be easily undercooled at low cooling rate into a glass.

The crystallization kinetics of the first crystallization step has been analyzed by using Kissinger's equation¹⁴

$$\beta/T_p^2 = (Zk_B/E_a)\exp(-E_a/k_B T_p), \quad (1)$$

where β is the heating rate, T_p is the crystallization peak temperature, Z is the frequency factor, k_B the Boltzmann constant and E_a the apparent activation energy. The Kissinger plots and the crystallization rate constant, K_{cr} , determined from the Arrhenius law

$$K_{cr}(T_p) = Z \exp(-E_a/k_B T_p), \quad (2)$$

are shown in Fig. 2. As expected, the values of the apparent activation energy and the frequency factor of the first crystallization stage rise in the same order as the crystallization onset temperature (see Table I). The rate constant is smaller for the alloy with the larger supercooled liquid region, similar as it was found for ZrTiCuNiFeBe ¹⁵ and FeNbAlGaPCB ¹⁶ metallic glasses with different compositions. The opposite tendency was reported for FeCoAlGaPCB alloys,¹⁷ for which the partial replacement of Co by Fe causes a decrease of K_{cr} and ΔT_x .

The dependence of the glass transition temperature on the heating rate β was evaluated in terms of the Vogel-Fulcher-Tamman (VFT) equation written in the form¹⁰

TABLE I. Glass transition temperature T_g , crystallization onset temperature T_x , liquidus temperature T_l , equilibrium solidification structure, activation energy E_a , and frequency factor Z of the first crystallization step for $\text{Co}_{62-x}\text{Fe}_x\text{Nb}_6\text{Zr}_2\text{B}_{30}$ ($x=0,16$) amorphous alloys (heating rate 0.17 K/s).

x	T_g (K)	T_x (K)	T_l (K)	T_g/T_l	Structures	E_a (eV)	Z (s ⁻¹)
0	900±5	950±1	1436±5	0.63±0.01	Eutectic	5.2±0.2	2×10 ²⁵
16	892±5	980±1	1420±5	0.63±0.01	Near-eutectic	6.1±0.2	4×10 ²⁹

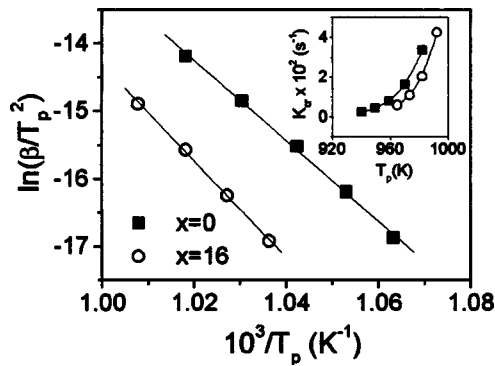


FIG. 2. Kissinger plots for $\text{Co}_{62-x}\text{Fe}_x\text{Nb}_6\text{Zr}_2\text{B}_{30}$ ($x=0,16$) amorphous alloys. The inset shows the temperature dependence of the crystallization rate constant K_{cr} .

$$\beta(T_g) = B \exp[DT_g^0 / (T_g^0 - T_g)], \quad (3)$$

where T_g^0 is the asymptotic value of T_g usually approximated as the onset of the glass transition within the limit of infinitely slow cooling and heating rate, B has the dimension of a heating rate and D is the strength parameter.

Figure 3 shows the DSC traces of the glass transition region of the studied alloys at heating rates from 0.02 to 2.67 K/s. Prior to the DSC scan, the as-quenched samples were preheated to above T_g and cooled to room temperature at 0.67 K/s, in order to achieve a relaxed glassy state for all the samples. The fitting of the experimental data was performed by the equation

$$\ln \beta(T_g) = \ln B - \frac{DT_g^0}{(T_g - T_g^0)} \quad (4)$$

with three adjustable VFT parameters: B , D , and T_g^0 . The calculated values are given in Table II and the best fits are shown by lines in Fig. 4(a). In order to compare the temperature dependence of the inverse heating rate $1/\beta$, for the two alloys, the inverse T_g scale has been normalized by T_g^* (the glass transition at the lowest heating rate of 0.02 K/s). At this heating rate, T_g^* is close to the temperature where the equilibrium viscosity is 10^{12} Pas.⁸ The experimental points and

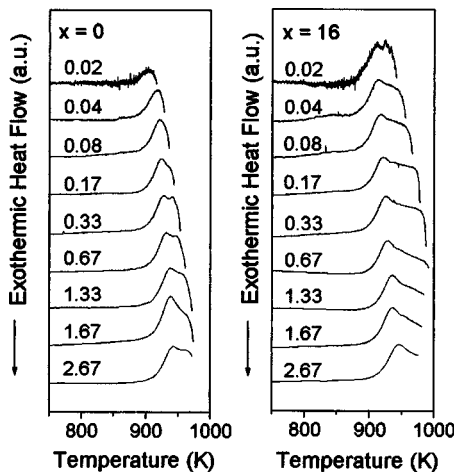


FIG. 3. DSC curves for $\text{Co}_{62-x}\text{Fe}_x\text{Nb}_6\text{Zr}_2\text{B}_{30}$ ($x=0,16$) alloys at different heating rates (in K/s).

TABLE II. VFT parameters for the best fit of the DSC data according to Eq. (4), and fragility m of $\text{Co}_{62-x}\text{Fe}_x\text{Nb}_6\text{Zr}_2\text{B}_{30}$ ($x=0,16$) glasses.

x	$\ln B(\text{K/s})$	D	$T_g^0(\text{K})$	T_g^*/T_g^0	m
0	20 ± 20	3 ± 2	760 ± 40	1.2 ± 0.2	44 ± 10
16	25 ± 20	7 ± 2	690 ± 40	1.3 ± 0.2	44 ± 10

the VFT fits are displayed in Fig. 4(b). The values obtained for the strength parameter, $D=3$ for $\text{Co}_{62}\text{Nb}_6\text{Zr}_2\text{B}_{30}$ and $D=7$ for $\text{Co}_{45}\text{Fe}_{16}\text{Nb}_6\text{Zr}_2\text{B}_{30}$ are of the same order of magnitude as the values found for $\text{Fe}(\text{Co})\text{Al}(\text{Si})\text{GaPCB}$ amorphous alloys.^{16,17} The decrease of the lower limit of the glass transition T_g^0 , and the increase of the strength parameter D with the substitution of Co by Fe, point in the same direction as the increase in the width of the supercooled liquid region (Table II).

The fragility concept provides a measure of the sensitivity of the structure of the liquid to temperature changes^{7,9} and can be used to classify glass-forming materials into three general categories: strong, intermediate and fragile.⁷ The fragility can be quantified by the strength parameter D in Eq. (3), which expresses the deviation from the Arrhenius behavior⁷ or by the fragility parameter defined as¹⁸

$$m = \left. \frac{d \log(\tau)}{d(T_g/T)} \right|_{T=T_g}, \quad (5)$$

where T is the temperature, T_g the glass transition, and $\langle \tau \rangle$ is the average relaxation time. From the VFT fits the fragility parameter at a particular T_g can be calculated according to⁹

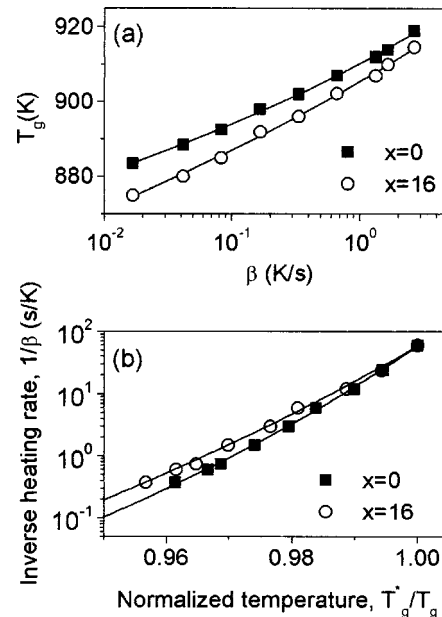


FIG. 4. Experimental points and VFT fits (lines) of (a) glass transition temperature T_g , as a function of the heating rate β , and (b) inverse heating rate $1/\beta$, as a function of inverse glass transition temperature $1/T_g$, normalized to $1/T_g^*$ (T_g^* : onset of the glass transition at 0.02 K/s), for $\text{Co}_{62-x}\text{Fe}_x\text{Nb}_6\text{Zr}_2\text{B}_{30}$ ($x=0,16$) alloys.

$$m = \frac{DT_g^0 T_g}{(T_g - T_g^0)^2 \ln 10}. \quad (6)$$

Open network liquids like SiO_2 and GeO_2 , that show an Arrhenius-type temperature dependence of relaxation times, provide the strong liquid extreme exhibiting values of m in the range $16 \leq m \leq 30$. In contrast, fragile liquids, such as ionic melts and polymers, which are characterized by simple nondirectional Coulomb attractions or by Van der Waals interactions exhibit large values of m (≥ 100). Since m is a measure of the steepness of the viscosity curve as a function of temperature at T_g , its value depends on the definition of T_g . In order to make a uniform comparison with fragility values found in the literature, m has been evaluated at T_g corresponding to a heating rate of 0.33 K/s. For both systems a value of 44 was found (Table II). Therefore, the significant increase in the width of the supercooled liquid region of about 40 K caused by the substitution of Co by Fe is not reflected in a change in the fragility parameter.

A value of $m=44$ indicates that the present alloys fall into the intermediate category according to Angell's classification scheme, and are closer to the strong limit than to the fragile limit. The same conclusions was stated for very good glass forming liquids such as $\text{Zr}_{46.75}\text{Ti}_{8.25}\text{Cu}_{7.4}\text{Ni}_{10}\text{Be}_{27.5}$ (Vitrealloy 4) ($m=34$, Refs. 8 and 19), $\text{Mg}_{65}\text{Cu}_{25}\text{Y}_{10}$ ($m=41$, Refs. 19 and 20), $\text{Pd}_{40}\text{Cu}_{30}\text{Ni}_{10}\text{P}_{20}$ ($m=52$, Refs. 19 and 21) and $(\text{Fe}_x\text{Co}_y\text{B}_z\text{Cu}_u)_{80}\text{Si}_3\text{Al}_5\text{Ga}_2\text{P}_{10}$ with $x=5-70$, $y=0-63$, $z=5-12$, and $u=0-5$ ($m=35$, Ref. 17). Therefore, it seems that there is a general correlation between improved glass-forming ability and stronger metallic liquids, as previously suggested.^{8,19} However, the fragility parameter m cannot be considered as a quantitative indicator to classify amorphous alloys in terms of their glass-forming ability, as it is not directly correlated to the critical cooling rate R_c for glass formation, that is, a lower fragility parameter does not imply a lower value of R_c . Thus, the critical cooling rates for some of the mentioned alloys are 30 K/s for the $\text{Zr}_{46.75}\text{Ti}_{8.25}\text{Cu}_{7.4}\text{Ni}_{10}\text{Be}_{27.5}$ (Ref. 22), 50 K/s for $\text{Mg}_{65}\text{Cu}_{25}\text{Y}_{10}$ (Ref. 20), and 0.1 K/s for $\text{Pd}_{40}\text{Cu}_{30}\text{Ni}_{10}\text{P}_{20}$ (Ref. 23).

Figure 5(a) shows the XRD patterns of the $\text{Co}_{62-x}\text{Fe}_x\text{Nb}_6\text{Zr}_2\text{B}_{30}$ ($x=0,16$) alloys at the beginning of the crystallization process. The samples were heated at 0.17 K/s up to 953 K ($x=0$) and 979 K ($x=16$), respectively. The structure of these crystallized samples consists of a residual amorphous phase + fcc $\text{Co}_{21}\text{Nb}_2\text{B}_6$ + orthorhombic $\text{CoNb}(\text{Zr})\text{B}$ + tetragonal Co_2B for the alloy with $x=0$, and amorphous phase + fcc $(\text{Co,Fe})_{21}\text{Nb}_2\text{B}_6$ + rhombohedral Co_3ZrB_2 + tetragonal $(\text{Co,Fe})_2\text{B}$ for $x=16$. In both cases three crystalline phases precipitate simultaneously. Therefore, it can be concluded that the high stability of the supercooled liquid is caused by the complicated crystallization reaction that requires a high degree of rearrangement of the constituents. The difference of the crystalline structures seems to be the reason for the different thermal stability of both supercooled liquids. Figure 5(b) shows the XRD patterns of $\text{Co}_{62-x}\text{Fe}_x\text{Nb}_6\text{Zr}_2\text{B}_{30}$ ($x=0,16$) samples heated at 0.17 K/s up to 1035 K, the temperature that corresponds to the end of the first crystallization step for both alloys. While

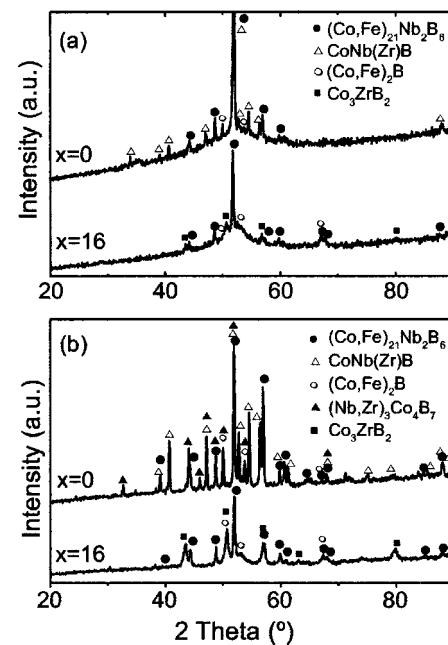


FIG. 5. XRD patterns corresponding to samples of $\text{Co}_{62-x}\text{Fe}_x\text{Nb}_6\text{Zr}_2\text{B}_{30}$ ($x=0,16$) alloys (a) heated at 0.17 K/s up to the beginning of the crystallization (953 K for $x=0$ and 979 K for $x=16$), and (b) heated up to the end of the first crystallization step (1035 K).

the same crystalline phases are found for $x=16$, new diffraction peaks corresponding to the orthorhombic $(\text{Nb,Zr})_3\text{Co}_4\text{B}_7$ phase are identified for the Fe-free sample. The crystallization of this new phase can be associated to the second weak exotherm, which follows the first strong DSC peak (Fig. 1).

The $\text{Co}_{46}\text{Fe}_{16}\text{Nb}_6\text{Zr}_2\text{B}_{30}$ as-quenched alloy exhibits good soft magnetic properties with a coercive field of 1.0 A/m, a saturation magnetization of 3.3×10^5 A/m ($\mu_0 M = 0.42$ T), a saturation magnetostriction of 1.1×10^{-6} and Curie temperature of 430 K, while the Fe-free alloy does not show ferromagnetic order at room temperature.

A thermomagnetic study of the crystallized samples at different stages of the crystallization process was made in order to support and complement the phase composition analysis of the crystallized alloys made by XRD. This study revealed that the composition of the crystalline phases changes as the crystallization progresses. Figure 6 shows the thermomagnetic curves at 0.17 K/s of crystallized

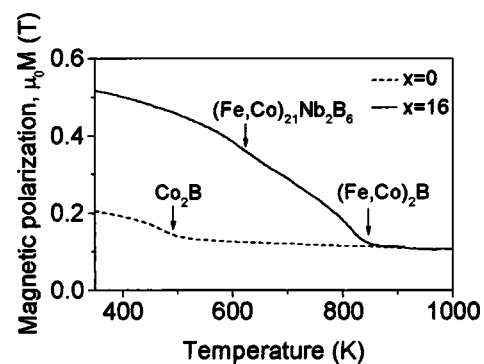


FIG. 6. Thermomagnetic curves, at 0.17 K/s, for $\text{Co}_{62-x}\text{Fe}_x\text{Nb}_6\text{Zr}_2\text{B}_{30}$ ($x=0,16$) samples preheated at 0.17 K/s up to 1073 K.

$\text{Co}_{62-x}\text{Fe}_x\text{Nb}_6\text{Zr}_2\text{B}_{30}$ ($x=0,16$) samples (preheated up to the end of the first crystallization process). The Curie transitions of some crystalline phases are marked with arrows. A Curie temperature of about 840 K for the $(\text{Fe},\text{Co})_2\text{B}$ phase, present in the alloy with $x=16$, indicates²⁴ that at the end of the first exotherm the Fe and Co contents of this phase are almost equal. A nonzero value of the magnetization at high temperatures (850 to 1000 K) for both alloys, is to be attributed to the presence of some traces of fcc Co(Fe) phase, the XRD peaks of which overlap with those of the $(\text{Co},\text{Fe})_{21}\text{Nb}_2\text{B}_6$ phase.

IV. CONCLUSIONS

The glass-forming ability of $\text{Co}_{62-x}\text{Fe}_x\text{Nb}_6\text{Zr}_2\text{B}_{30}$ ($x=0,16$) amorphous alloys with large supercooled liquid region was analyzed in terms of the width of the supercooled liquid region, the reduced glass transition temperature and the Vogel–Fulcher–Tamman parameters. A value of the fragility parameter of 44 indicates that the present alloys fall into the intermediate category according to Angell's classification scheme, being closer to the strong limit than to the fragile limit. The significant increase in the width of the supercooled liquid region of about 40 K caused by the substitution of Co by Fe is not accompanied by a change in the fragility parameter. The high stability of the supercooled liquid is caused by the complicated crystallization reaction that requires a high degree of rearrangement of the constituents. The $\text{Co}_{46}\text{Fe}_{16}\text{Nb}_6\text{Zr}_2\text{B}_{30}$ alloy exhibits good soft magnetic properties, while the Fe-free alloy does not show ferromagnetic order at room temperature.

ACKNOWLEDGMENTS

This work was partially supported by the Spanish Ministry of Science and Technology and EU-FEDER (Project

MAT2001-3175), by the PAI of the Junta de Andalucía, and by the EU (RTN-Network on "Bulk Metallic Glasses," Contract HPRN-CT-2000-00033). One of the authors (J. M. B.) acknowledges the IFW Dresden and the Junta de Andalucía for research fellowships.

¹A. Inoue, *Acta Mater.* **48**, 279 (2000).

²A. Inoue, A. Makino, and T. Mizushima, *J. Magn. Magn. Mater.* **215–216**, 246 (2000).

³A. Inoue, T. Itoi, K. Koshiba, and A. Makino, *IEEE Trans. Magn.* **35**, 3355 (1999).

⁴A. Inoue, A. Takeuchi, and B. Shen, *Mater. Trans., JIM* **42**, 970 (2001).

⁵T. Itoi and A. Inoue, *Appl. Phys. Lett.* **74**, 2510 (1999).

⁶T. Itoi and A. Inoue, *Mater. Trans., JIM* **41**, 1256 (2000).

⁷C. A. Angell, *Science* **267**, 1924 (1995).

⁸R. Busch, E. Bakke, and W. L. Johnson, *Acta Mater.* **13**, 4725 (1998).

⁹R. Böhmer, K. L. Ngai, C. A. Angell, and D. J. Plazek, *J. Chem. Phys.* **99**, 4201 (1993).

¹⁰R. Brüning and K. Samwer, *Phys. Rev. B* **46**, 11318 (1992).

¹¹K. Narita, J. Yamasaki, and H. Fukunaga, *IEEE Trans. Magn.* **16**, 435 (1980).

¹²Z. P. Lu, H. Tan, Y. Li, and S. C. Ng, *Scr. Mater.* **42**, 667 (2000).

¹³D. Turnbull, *Contemp. Phys.* **10**, 473 (1969).

¹⁴H. E. Kissinger, *J. Res. Natl. Bur. Stand., Sect. A* **57**, 217 (1956).

¹⁵Y. X. Zhuang, W. H. Wang, Y. Zhang, M. X. Pan, and D. Q. Zhao, *Appl. Phys. Lett.* **75**, 2392 (1999).

¹⁶N. Mitrovic, S. Roth, and J. Eckert, *Appl. Phys. Lett.* **78**, 2145 (2001).

¹⁷J. M. Borrego, A. Conde, S. Roth, and J. Eckert, *J. Appl. Phys.* **92**, 2073 (2002).

¹⁸R. Böhmer and C. A. Angell, *Phys. Rev. B* **45**, 10091 (1992).

¹⁹D. N. Perera and A. P. Tsai, *J. Phys. D* **33**, 1937 (2000).

²⁰R. Busch, W. Liu, and W. L. Johnson, *J. Appl. Phys.* **83**, 4134 (1998).

²¹H. Kato, Y. Kawamura, A. Inoue, and H. S. Chen, *Appl. Phys. Lett.* **73**, 3665 (1998).

²²T. A. Waniuk, J. Schroers, and W. L. Johnson, *Appl. Phys. Lett.* **78**, 1213 (2001).

²³A. Inoue, N. Nishiyama, and T. Masumoto, *Mater. Trans., JIM* **37**, 181 (1996).

²⁴O. Beckman and L. Lundgren, *Handbook of Magnetic Materials*, edited by K. H. J. Buschow (Elsevier, Amsterdam, 1991), Vol. 6, p. 218.